Nutrient Utilisation and Weathering Inputs in the Peruvian Upwelling Region Since the Little Ice Age

C. Ehlert[1,*], P. Grasse[1], D. Gutiérrez[2], R. Salvatteci[2,3] and M. Frank[1]

[1] GEOMAR Helmholtz Centre for Ocean Research Kiel, Germany

[2] Instituto del Mar del Perú (IMARPE), Dirección de Investigaciones Oceanográficas, Callao, Peru

[3] Institute of Geoscience, Department of Geology, Kiel University, Ludewig-Meyn-Str. 10 D-24118 Kiel, Germany

[*] now at: Max Planck Research Group for Marine Isotope Geochemistry, Institute for Chemistry and Biology of the Marine Environment (ICBM), University of Oldenburg

Correspondence to: C. Ehlert (cehlert@mpi-bremen.de)

Keywords:

stable silicon isotopes, stable nitrogen isotopes, primary productivity, river input, eolian input, material transport, Little Ice Age, nutrient utilisation

Abstract

For this study two sediment cores from the Peruvian shelf covering the time period between the Little Ice Age (LIA) and present were examined for changes in productivity (biogenic opal concentrations (bSi)), nutrient utilisation (stable isotope compositions of silicon ($\delta^{30}Si_{opal}$) and nitrogen ($\delta^{15}N_{sed}$)), as well as in ocean circulation and material transport (authigenic and detrital radiogenic neodymium (ε_{Nd}) and strontium ($^{87}Sr/^{86}Sr$) isotopes).

For the LIA the proxies recorded weak primary productivity and nutrient utilisation reflected by low average bSi concentrations of ~10%, $\delta^{15}N_{sed}$ values of ~5‰ and intermediate $\delta^{30}Si_{opal}$ values of ~0.9‰. At the same time the radiogenic isotope composition of the detrital sediment

fraction indicates dominant local riverine input of lithogenic material due to higher rainfall in the Andean hinterland. These patterns were most likely caused by permanent El Niño-like conditions characterized by a deeper nutricline, weak upwelling and low nutrient supply. At the end of the LIA, $\delta^{30}Si_{opal}$ dropped to low values of +0.6‰ and opal productivity reached its minimum of the past 650 years. During the following transitional period of time the intensity of upwelling, nutrient supply and productivity increased abruptly as marked by the highest bSi contents of up to 38%, by $\delta^{15}N_{sed}$ of up to ~7‰, and by the highest degree of silicate utilisation with $\delta^{30}Si_{opal}$ reaching values of +1.1‰. At the same time detrital ε_{Nd} and $^{87}Sr/^{86}Sr$ signatures documented increased wind strength and supply of dust to the shelf due to drier conditions. Since about 1870, productivity has been high but nutrient utilisation has remained at levels similar to the LIA indicating significantly increased nutrient availability.

Comparison between the $\delta^{30}Si_{opal}$ and $\delta^{15}N_{sed}$ signatures suggests that during the past 650 years the $\delta^{15}N_{sed}$ signature in the Peruvian Upwelling area has to a large extent been controlled by surface water utilisation and not, as previously assumed, by subsurface nitrogen loss processes in the water column, which only had a significant influence during modern times (i.e. since ~1870 AD).

1 Introduction

Global climate of the late Holocene was disrupted by major anomalies, the most recent of which being the Little Ice Age (LIA) between ca. 1400 and 1850 AD (Lamb, 1965; Grove, 2001). During that time a weakening of the Walker circulation (Conroy et al., 2008), reduced influence of the South Pacific subtropical high (SPSH) along the Peruvian margin (Sifeddine et al., 2008; Gutiérrez et al., 2009; Salvatteci et al., 2014a), and a southward shift of the mean position of the Intertropical Convergence Zone (ITCZ) and the associated precipitation belt compared to today (Sachs et al., 2009) caused pronounced changes in rainfall patterns in the tropics. El Niño-like warmer conditions in the Eastern South Pacific were accompanied by an intensified South American summer monsoon (Bird et al., 2011) resulting in ~10% higher precipitation in northeast Peru (~5°S; Rabatel et al., 2008) and up to 20-30% higher precipitation in the Bolivian Andes (~16°S; Reuter et al., 2009). On the one hand this caused growth and extension of the Andean glaciers (Vuille et al., 2008) and on the other it enabled human settlements in the presently hyperarid southern Peruvian Andes (Unkel et al., 2007). In

the upwelling areas off Peru and the western South American shelf regions the main consequence of these climatic conditions during the LIA was a deepening of the nutricline and a strongly diminished biological productivity (Vargas et al., 2007; Sifeddine et al., 2008; Valdés et al., 2008; Gutiérrez et al., 2009).

Sediment cores from the Peruvian shelf covering the period of time from the LIA until present indicate that the marine realm was characterised by an abrupt biogeochemical regime shift towards modern conditions at the end of the LIA due to the northward movement of the ITCZ and an expansion of the SPSH. While low productivity and a more oxygenated water column prevailed during the LIA, markedly increased biological productivity and pronounced oxygen depletion over wide areas of the shelf have characterised the system since the end of the LIA (Vargas et al., 2007; Sifeddine et al., 2008; Gutiérrez et al., 2009, Salvatteci et al., 2014a).

In this study the stable silicon isotope composition of sedimentary diatoms ($\delta^{30}Si_{opal}$) covering the period of time from the LIA to the present is analysed. The main goal is the reconstruction of the factors controlling the dynamics of nutrient cycling together with oxygen in the Peruvian upwelling, in particular a comparison between the $\delta^{30}Si_{opal}$ and the stable nitrogen isotope composition ($\delta^{15}N_{sed}$) of sedimentary organic matter. Both $\delta^{30}Si_{opal}$ and $\delta^{15}N_{sed}$ provide information about utilisation of silicic acid ($Si(OH)_4$) and nitrate (NO_3^-) during primary productivity, e.g. during the formation of diatom frustules and associated organic matter, respectively (Altabet and Francois, 1994; De La Rocha et al., 1997). Diatoms preferentially incorporate the lighter isotopes from the dissolved $Si(OH)_4$ and NO_3^- pools leaving the residual dissolved nutrients enriched in the heavier isotopes (Wada and Hattori, 1978; Altabet et al., 1991; De La Rocha et al., 1997). Si isotope fractionation is mainly controlled by the utilisation of $Si(OH)_4$ in surface waters by biota (diatoms) (e.g., De La Rocha et al., 1998; Brzezinski et al., 2002; Egan et al., 2012). The $\delta^{15}N$ of NO_3^- is partly controlled by NO_3^- utilisation of marine organisms but is also affected by N-loss processes in the water column (denitrification, anammox) (Codispoti et al., 2001; Dalsgaard et al., 2003) resulting in a marked enrichment of the upwelling source waters in the heavier $^{15}NO_3^-$ (Liu and Kaplan, 1989; Lam et al., 2009; given that it is currently not possible to distinguish between different N-loss processes from the sediments we will use the term denitrification for simplicity). Consequently, sedimentary $\delta^{15}N_{sed}$ records from areas dominated by oxygen-depleted waters such as the shelf region off Peru are usually interpreted to directly reflect changes in the intensity of subsurface NO_3^- loss and the extent and strength of oxygen

depletion (e.g., De Pol-Holz et al., 2007, 2009; Agnihotri et al., 2008; Gutiérrez et al., 2009) whereas the effect of NO_3^- utilisation on the preserved $\delta^{15}N_{sed}$ is often neglected. Comparison of both isotope systems can therefore provide information about the degree of utilisation of NO_3^- and $Si(OH)_4$ versus the influence of NO_3^- loss processes. Increasing nutrient utilisation should result in a consistent increase in both $\delta^{30}Si_{opal}$ and $\delta^{15}N_{sed}$. In contrast, a change in NO_3^- reduction due to varying oxygen depletion in the water column would affect only the $\delta^{15}N_{sed}$ leaving the $\delta^{30}Si_{opal}$ unaffected.

The main forces driving surface productivity and subsurface oxygenation off Peru at centennial time scales during the past two millennia have been changes in the strength of the Walker circulation and in the expansion/contraction of the SPSH (Gutierrez et al., 2009; Salvatteci et al., 2014a). Therefore, the radiogenic isotope compositions of neodymium (ε_{Nd}) and strontium ($^{87}Sr/^{86}Sr$) of the authigenic ferromanganese (Fe-Mn) oxyhydroxide coatings of the sedimentary particles, which are expected to record the radiogenic isotope compositions of past bottom waters, as well as of the detrital fraction of the sediment were examined. These proxy data provide information about changes of (surface ocean) circulation and of transport processes, provenance of the sediments, and input mechanisms of terrigenous material as a function of changes in precipitation on land during the transition from wetter LIA-conditions to drier modern conditions. Weathering of continental source rocks delivers lithogenic particles of different origin and age to the shelf, which have distinct radiogenic isotope signatures ($\varepsilon_{Nd\ detritus}$, $^{87}Sr/^{86}Sr_{detritus}$) that can be used to trace their source areas (Goldstein et al., 1984). Central Peruvian Andean rocks have more radiogenic ε_{Nd} signatures whereas southern Peruvian rocks are characterised by less radiogenic ε_{Nd} signatures (Sarbas and Nohl, 2009), which is also reflected in the sediments along the shelf (Ehlert et al., 2013). Changes in detrital material input and transport pathways are generally closely related to climatic changes causing variations in the supply from the respective source areas (e.g. Grousset et al., 1988). It should therefore be possible to detect the transition from wetter LIA-conditions with higher local input from central Peru via rivers due to higher precipitation rates towards the drier presently prevailing conditions with an increased influence of eolian material transport from further south in the Atacama desert (Molina-Cruz, 1977) and deposition along the shelf after the LIA.

2 Material and Methods

2.1 Core Locations and Age Models

For the reconstruction of surface water $Si(OH)_4$ utilisation and terrestrial material input and transport for the period of time between the LIA and present two sediment cores with high sedimentation rates were analysed. Box core B0405-6 was recovered from the upper continental slope off Pisco at 14°07.9' S, 76°30.1' W in a water depth of 299 m with the Peruvian R/V José Olaya Balandra in 2004 (Fig. 1) (Gutiérrez et al., 2006). The age model was previously published by Gutiérrez et al. (2009) and is based on downcore profiling of the activities of ^{241}Am, excess ^{210}Pb, and on radiocarbon ages obtained from bulk sedimentary organic carbon, which document that the core covers the past ~650 years. The second core, multicorer M771-470, was taken at 11° S, 77°56.6' W in 145 m water depth during cruise M77/1 with the German R/V Meteor in 2008 (Fig. 1). The age model was obtained by measuring excess ^{210}Pb activities and modeling of the resulting profiles as described by Meysman et al. (2005) (for details see Supplement). Ages prior to ~1850 AD were inferred using sedimentation rates from nearby core B0405-13 (Gutiérrez et al., 2009; Salvatteci et al., 2014b).

2.2 Methods

2.2.1 Biogenic Opal and Silicon Isotope Analyses

The biogenic opal (bSi) contents in both cores were measured following the sequential leaching techniques described by DeMaster (1981) and Müller and Schneider (1993). Si isotope analyses were performed on the 11-32μm diatom-fraction that was extracted from the sediment applying the procedures described by Morley et al. (2004).

Approximately 300 mg of sediment were treated with 30% H_2O_2 and 35% HCl to remove organic matter and carbonate. Afterwards the sediment was wet-sieved to separate the 11-32 μm fraction. In a third step a heavy-liquid solution (sodium-polytungstate, 2.1-2.2 g/mL) was applied in several steps to separate diatoms from the detrital lithogenic silicate material. All samples were screened under the microscope to verify their purity with respect to the detrital (clay) fraction.

The diatom samples were then transferred into Teflon vials and dissolved in 1 mL 0.1 M

NaOH and diluted with MQ water according to Reynolds et al. (2008). More details are provided in Ehlert et al. (2012). Si concentrations of the dissolved diatom samples were measured colorimetrically using a photospectrometer (Hansen and Koroleff, 1999). Chromatographic separation and purification of the Si was achieved with 1mL pre-cleaned AG50W-X8 cation exchange resin (mesh 200-400) (Georg et al., 2006; as modified by de Souza et al., 2012). Si isotope ratios were measured on a *NuPlasma HR* MC-ICPMS (Nu Instruments) at GEOMAR equipped with an adjustable source-defining slit, which can be set to medium resolution to ensure separation of the ^{30}Si peak from molecular interferences. The measurements were carried out applying standard-sample bracketing (Albarède et al., 2004). All solutions were measured at a Si concentration of 14-21 µmol/kg of samples and standards depending on the performance of the instrument on the respective measurement day and were introduced into the plasma via a Cetac Aridus II desolvating nebulizer system equipped with a PFA nebulizer operated at a 60 to 80 µL/min uptake rate. Si isotope compositions are reported in the $\delta^{30}Si$ notation as deviations of the measured $^{30}Si/^{28}Si$ from the NIST standard NBS28 in parts per thousand (‰). Repeated measurements of the reference materials IRMM018 and Big Batch gave average $\delta^{30}Si$ values of -1.52 ± 0.18‰ ($2\sigma_{(sd)}$) and -10.84 ± 0.18‰ ($2\sigma_{(sd)}$), respectively, which are in good agreement with values obtained by other laboratories (Reynolds et al., 2007). Samples were measured three to five times within a one-day session and measurements were repeated on at least two separate days. The resulting uncertainties ranged between 0.04 and 0.23‰ ($2\sigma_{(sd)}$) (Tables 1, 2). Replicate measurements of an in-house diatom matrix standard over longer periods of time gave an external reproducibility of 0.11‰ ($2\sigma_{(sd)}$). Error bars provided in the figures correspond to that external reproducibility unless the uncertainties of the repeated sample measurements were higher.

2.2.2 Neodymium and Strontium Isotope Analyses

To obtain the radiogenic isotope composition of past bottom seawater at the sites of the sediment cores from the early diagenetic Fe-Mn coatings of the sediment particles, previously published methods were applied (Gutjahr et al., 2007; see supplement for details). The residual detrital material was leached repeatedly to remove remaining coatings and was then treated with a mixture of concentrated HF-HNO_3-HCl for total dissolution. The separation and purification of Nd and Sr in the leachates and in the completely dissolved detrital

sediment fraction followed previously published procedures for Nd (Cohen et al., 1988) and Sr (Horwitz et al., 1992) applying ion exchange chromatography for separation of Rb/Sr from the rare earth elements (REEs) (0.8 mL AG50W-X12 resin, mesh 200-400) followed by separation of Sr from Rb (50 µL Sr-Spec resin, mesh 50-100), and separation of Nd from the other REEs (2 mL Eichrom Ln-Spec resin, mesh 50-100). All radiogenic isotope measurements were performed on the *NuPlasma HR* MC-ICPMS (Nu Instruments) at GEOMAR. Measured Nd isotope compositions were corrected for instrumental mass bias using a $^{146}Nd/^{144}Nd$ of 0.7219 and were normalised to the accepted $^{143}Nd/^{144}Nd$ literature value of 0.512115 of the JNdi-1 standard (Tanaka et al., 2000). All values are given as ε_{Nd}, which corresponds to the measured $^{143}Nd/^{144}Nd$, normalised to the Chondritic Uniform Reservoir CHUR (0.512638), multiplied by 10,000. The external reproducibility was estimated by repeated measurements of the JNdi-1 standard and was always better than 20 ppm ($2\sigma_{(sd),}$ Tables 1, 2). Measured $^{87}Sr/^{86}Sr$ ratios were corrected for instrumental mass bias using $^{88}Sr/^{86}Sr = 8.3752$ and were normalised to the accepted value for NIST SRM987 of 0.710245. The $2\sigma_{(sd)}$ external reproducibility of repeated standard measurements was always better than 36 ppm ($2\sigma_{(sd),}$ Tables 1, 2). Procedural Nd and Sr blanks for leachates and total dissolutions of the detrital material were ≤ 83 pg and 2.1 ng, respectively, and thus negligible compared to the concentrations of the samples.

3 Results

3.1 Core M771-470 (Callao)

Sediment core M771-470 located at 11°S in 145 m water depth, is characterised by bSi concentrations between 10.1% and 26.9% and total N contents between 0.5% and 1.1% (Fig. 2a, Table 1), whereby the lowest values occurred just prior to the end of the LIA. The maximum bSi concentrations were found during the transition period. In contrast, the highest nitrogen (N) content occurred later in the youngest part of the record. The $\delta^{30}Si_{opal}$ varied between +0.6‰ and +1.1‰ (Fig. 2b) and followed bSi concentrations with the maximum and minimum isotope values corresponding to the same respective depths for both parameters.

The $\varepsilon_{Nd\ detritus}$ is characterised by values between -3.6 and -5.2 with a mean value of -4.5 ± 1.0 ($2\sigma_{(sd)}$) (Fig. 2c, Table 1). The $^{87}Sr/^{86}Sr_{detritus}$ signatures of the same samples range between 0.70647 and 0.70936 (Fig. 2d, Table 1). The variability of $\varepsilon_{Nd\ detritus}$ and $^{87}Sr/^{86}Sr_{detritus}$ is very

similar. Samples from the LIA show a trend towards more radiogenic $\varepsilon_{Nd\ detritus}$ and less radiogenic $^{87}Sr/^{86}Sr_{detritus}$. At the beginning of the transition period both records indicate a marked change to less radiogenic $\varepsilon_{Nd\ detritus}$ and more radiogenic $^{87}Sr/^{86}Sr_{detritus}$ values, which was more pronounced in the Sr than in the Nd isotope data, resulting in the youngest samples having the least radiogenic $\varepsilon_{Nd\ detritus}$ and the most radiogenic $^{87}Sr/^{86}Sr_{detritus}$ signatures.

In theory, the radiogenic isotope composition of authigenic Fe-Mn oxyhydroxide coatings is a useful tracer to detect changes on the prevailing bottom water masses at a distinct location. The PCUC, which dominates the bottom waters at the core locations today, is characterised by radiogenic ε_{Nd} signatures of -1.8 (Lacan and Jeandel, 2001; Grasse et al., 2012). A deepening of the nutricline and a vertical expansion of surface water masses during the LIA could change that value towards less radiogenic signatures typical for water masses originating from the South Pacific (Piepgras and Wasserburg, 1982; Grasse et al., 2012). However, as shown before (Ehlert et al., 2013) the authigenic coating fraction from sediments along the Peruvian shelf does not necessarily represent changes in water mass advection and is therefore not a reliable proxy (see also Supplement for details).

3.2 Core B0405-6 (Pisco)

In core B0405-6 located near 14°S off Pisco in 299 m water depth the range of bSi concentrations and its maximum value are higher than in core M771-470 and varied between 12.6% and 37.7% (Fig. 2e, Table 2). The trends are very similar to those of core M771-470 and bSi content correlates closely with the diatom accumulation rate (Fig. 2e). The lowest values of both parameters occurred at the end of the LIA and highest values were found right after the end of the LIA at the beginning of the transition period. The N content ranges from 0.5% around 1860 AD to 1.8% in the youngest sample of the record (Fig. 2e) (Gutiérrez et al., 2009) with maximum N content in core B0405-6 also being higher than in core M771-470. The $\delta^{30}Si_{opal}$ record shows the same range from +0.6‰ to +1.1‰ as core M77/1-470 and a very similar trend with the lowest values near the end of the LIA and the highest values immediately thereafter during the transition period (Fig. 2f, Table 3). The $\delta^{15}N_{sed}$ ranges between 3.6‰ and 7.6‰ and shows a trend from lower mean values around 4‰ to 5‰ during the LIA to higher values between 6‰ and 7‰ in the modern sediments (Fig. 2f).

The $\varepsilon_{Nd\ detritus}$ signatures are characterised by overall somewhat more radiogenic values than of core M771-470 ranging from -4.1 to -2.5 (mean value -3.2 ± 0.9, $2\sigma_{(sd)}$ excluding the value of -0.2 ε_{Nd} at 1761 AD, which is considered an outlier), with slightly less radiogenic values in the older part of the record and more radiogenic values in the younger part (Fig. 2g, Table 2). The $^{87}Sr/^{86}Sr_{detritus}$ values range between 0.70711 and 0.70796 (Fig. 2h, Table 2). Similar to core M771-470 although less pronounced, the main feature in the detrital Sr isotope record observed is a trend from less radiogenic $^{87}Sr/^{86}Sr_{detritus}$ values in the older part of the record towards more radiogenic values in the youngest part with a shift at the end of the LIA and during the early transition period.

4 Discussion

After the end of the LIA around 1820 AD the mean position of the ITCZ shifted northward (Sachs et al., 2009) causing an intensification of alongshore winds and enhanced coastal upwelling off the Peruvian coast (Sifeddine et al., 2008; Gutiérrez et al., 2009), diminished coastal sea surface temperatures (Vargas et al., 2007), and a decrease in precipitation on land (Rabatel et al., 2008; Bird et al., 2011). Records of productivity and redox conditions based on $\delta^{15}N_{sed}$ and the Mo and Cd content of the sediments indicate a rapid change of the biogeochemical composition of the source waters to higher nutrient concentrations causing higher biological productivity and lower subsurface oxygen, which have persisted until the present day (Sifeddine et al., 2008; Gutiérrez et al., 2009; Salvatteci et al., 2014a). The shift after the end of the LIA constitutes a major anomaly of late Holocene climate in the Eastern Pacific, which was of the same order of magnitude as the changes in conditions off Chile during the Younger Dryas (De Pol-Holz et al., 2006). This study focuses on the reconstruction of the regime shift from the LIA and a transitional period towards modern conditions and its controlling factors including the evolution of nutrient utilisation and changes in the advection of water masses and material transport.

4.1 Changes in Biological Productivity and Nutrient Consumption

4.1.1 Evolution of Surface Water Productivity and Nutrient Utilisation

The pronounced change in the biogeochemical regime from low productivity during the LIA to higher productivity during the transitional and modern period thereafter is documented by several sedimentary records from the EEP region and has been dated at ~1820 AD (Sifeddine et al., 2008; Gutierrez et al., 2009; Díaz-Ochoa et al., 2009, 2011; Salvatteci et al., 2014a). Similarly, both cores M771-470 from 11°S and B0405-6 from 14°S off Pisco show the characteristic coeval pronounced increase in bSi and total N content (Figs. 2a, e) and C_{org} concentration (not shown here) after the end of the LIA and during the transition period. Therefore, three time periods that show distinct differences in productivity and nutrient utilisation have been identified from our records and will be discussed in the following: the LIA, the transition period from the LIA to modern conditions between ~1820 and ~1870AD, and modern conditions after ~1870 AD.

Both cores recorded a two- to threefold increase in bSi content from 10-12% prior to the end of the LIA to values of up to 27% in M771-470 and up to 38% in B0405-6 during the transition period (Figs. 2a, e). Afterwards the bSi contents decreased again but have remained at a level of ~20% and thus significantly higher than prior to the end of the LIA. The increase in bSi content is also reflected by a marked increase in diatom accumulation rate in core B0405-6 (Fig. 2e) (Gutiérrez et al., 2009). Analyses of the downcore diatom assemblages have shown that the high diatom accumulation rates and bSi content in core B0405-6 during the transition period were associated with diatom layers dominated by *Skeletonema costatum* (Gutiérrez et al., 2009), a species that is today more abundant when upwelling is more intense during Austral winter/spring.

Both cores are characterised by a very high correlation between total N and C_{org} content (r^2=0.95 for core M771-470 and 0.8 for core B0405-6, respectively) (Gutiérrez et al., 2009; this study). In contrast, bSi and total N contents do not co-vary throughout the records (Fig. 3a). Surface sediments from the Peruvian shelf region between the Equator and ~18°S show a relatively weak but positive correlation between bSi and N contents (r^2 = 0.5, Fig. 3a) (Ehlert et al., 2012; Mollier-Vogel et al., 2012). Similar to the surface sediments, bSi and total N concentrations in core M771-470 are positively correlated, whereas they essentially do not correlate in core B0405-6. This is because the bSi maximum at the end of the transition period was more pronounced in core B0405-6 and higher than surface sediment bSi contents anywhere along the shelf region off Peru. At the same time only a rather gradual increase in total N content with some excursions to low values during the transition period occured (Figs.

2a, e). The total N concentration also did not always co-vary with $\delta^{15}N_{sed}$ (Fig. 3c). In particular, the samples from the late transition period show very low total N concentrations but high $\delta^{15}N_{sed}$, high $\delta^{30}Si_{opal}$ and bSi content.

Sedimentary $\delta^{15}N_{sed}$ data, which are only available for core B0405-6, show a shift from lower values around +4‰ to +5‰ during the LIA to higher values around +7‰ after the end of the LIA and have remained at that level since then (Fig. 2f) (Gutiérrez et al., 2009). The values in the younger part of the record are in good agreement with surface sediment $\delta^{15}N_{sed}$ data measured in the main Peruvian upwelling region ranging from +6‰ to +9‰ (Mollier-Vogel et al., 2012). Bulk $\delta^{15}N_{sed}$ signatures measured in core B0405-13 from 12°S (184 m water depth) close to the location of core M771-470 can be used for comparison and show very similar values, amplitude, and variability as core B0405-6 (Fig. 2i) (Gutiérrez et al., 2009). In contrast to $\delta^{15}N_{sed}$, the $\delta^{30}Si_{opal}$ signatures, which mainly reflect changes in surface water nutrient utilisation, are not only characterised by a simple increase at the end of the LIA. Instead, both $\delta^{30}Si_{opal}$ records closely follow the evolution of the bSi concentrations and show intermediate $\delta^{30}Si_{opal}$ signatures between +0.8‰ and +0.9‰ during the LIA, a pronounced short-term decrease to +0.6‰ at the end of the LIA, which was followed by a marked increase to values around +1.1‰ during the transition period, and finally a return to intermediate values between +0.8‰ and +1.0‰ in the modern part of the records (Figs. 2b, f). The correspondence between bSi content and $\delta^{30}Si_{opal}$ is more pronounced in core B0405-6 (Fig. 3b), which shows a higher variability and amplitude of bSi content. The difference in the $\delta^{30}Si_{opal}$, $\delta^{15}N_{sed}$, bSi and total N content records during the transition from LIA to modern conditions reflects the different environmental factors controlling the proxies, which will be discussed in the following sections.

4.1.2 Present Day Surface Water Utilisation versus Subsurface Nitrate Loss

Diatoms are the dominant phytoplankton group of the Peruvian upwelling region (Estrada and Blasco, 1985; Bruland et al., 2005). The $\delta^{30}Si_{opal}$ of these diatoms is primarily controlled by surface water diatom productivity and $Si(OH)_4$ utilisation (De La Rocha et al., 1998; Brzezinski et al., 2002; Egan et al., 2012). Off Peru the $\delta^{30}Si_{opal}$ has also been shown to be dependent on the isotopic signature of the advected surface and subsurface water masses (Ehlert et al., 2012; Grasse et al., 2013). Similarly, the $\delta^{15}N_{sed}$ of the organic matter is

controlled by N isotope fractionation during NO_3^- uptake by phytoplankton, mostly diatoms. Off Peru, however, the NO_3^- supplied to the surface waters has previously been enriched in $^{15}NO_3^-$ due to upwelling of oxygen-depleted subsurface waters, which had undergone significant NO_3^--loss processes (mostly denitrification, but also anammox processes, associated with a high fractionation of up to 20-30‰) (Lam et al., 2009; Altabet et al., 2012). Bulk sediment $\delta^{15}N_{sed}$ in areas with oxygen-depleted waters is therefore usually interpreted to reflect changes in the intensity of subsurface NO_3^- reduction and the extent and strength of the oxygen minimum zone (Altabet et al., 1999; De Pol-Holz et al., 2007; Agnihotri et al., 2008; Gutiérrez et al., 2009). The direct comparison of $\delta^{30}Si_{opal}$, reflecting mostly utilisation, and $\delta^{15}N_{sed}$, reflecting both utilisation and NO_3^- reduction, from core B0405-6 off Pisco will therefore provide insights into the strength of NO_3^- reduction in the past.

Subsurface water column $\delta^{15}N_{NO3-}$ data from the present-day Peruvian shelf are isotopically very heavy, in particular along the southern shelf region between 10°S and 17°S, where values of up to +25‰ are reached due to the increasing oxygen deficit and intensification of NO_3^--loss processes (Mollier-Vogel et al., 2012; Altabet et al., 2012). These isotopically enriched waters are upwelled along the shelf and represent the source for organic matter production in the surface waters. Therefore, it is expected, that the deposited sedimentary organic matter reflects these enriched subsurface water signatures. However, the latitudinal increase in surface sediment $\delta^{15}N_{sed}$ from the same shelf region to maximum mean values around +9‰ is much lower than that measured in the water column (Mollier-Vogel et al., 2012). The reason for this observation is that the $\delta^{15}N_{sed}$ signal in the southern shelf region (10-17°S) did not fully record the the $^{15}NO_3^-$ enrichment in the water column but is a combination of the isotopic effects associated with subsurface NO_3^--loss and incomplete surface water NO_3^- utilisation and water mass mixing. Direct comparison of $\delta^{30}Si_{opal}$ and $\delta^{15}N_{sed}$ allows to investigate and to distinguish the relative importance of these processes (Fig. 4a). Diatoms off Peru preferentially take up $Si(OH)_4$ and NO_3^- at a ratio of ~1:1 or below (Brzezinski, 1985; Takeda, 1998; Hutchins et al., 2002). If utilisation were the only driving factor, the sedimentary $\delta^{30}Si_{opal}$ and $\delta^{15}N_{sed}$ should all plot close to a line that reflects the enrichment during increasing utilisation, i.e. 1.1‰ for $\delta^{30}Si_{opal}$ (De La Rocha et al., 1997) and ~5‰ for $\delta^{15}N$ (DeNiro and Epstein, 1981; Minagawa and Wada, 1984). Under the influence of denitrification with an enrichment of ~20‰ (Lam et al., 2009), however, the relationship between $\delta^{30}Si_{opal}$ and $\delta^{15}N_{sed}$ would be very different (Fig. 4a).

Most modern shelf samples plot either on or above the theoretical curve for utilisation implying, if at all, $Si(OH)_4$ limiting conditions (Fig. 4a). Very few samples are shifted towards the theoretical curve for denitrification, indicating a weak influence of NO_3^--loss processes on the preserved isotope signatures. Especially along the central shelf region (green curves in Fig. 4a), where the cores are located, surface sediment signatures closely reflect the utilisation in surface waters with only little influence of NO_3^--loss in the water column and sediments.

4.1.3 Past Surface Water Utilisation versus Subsurface Nitrate Loss

Assuming that source water isotope composition (+1.5‰ $\delta^{30}Si_{Si(OH)4}$, +9‰ $\delta^{15}N_{NO3}$) and isotope enrichment during utilisation and denitrification (-1.1‰ $\delta^{30}Si_{opal}$, ~-5‰ and ~-20‰ $\delta^{15}N_{NO3-}$ for utilisation and denitrification, respectively) in the past were similar to the conditions of the present-day shelf region (Ehlert et al., 2012; Mollier-Vogel et al. 2012), the samples of core B0405-6 indicate variable utilisation/NO_3^--loss conditions (Fig. 4b). Samples from the LIA and the transition period generally plot on or above the utilisation curve indicating stronger $Si(OH)_4$ than NO_3^- utilisation. This implies that in the Peruvian upwelling system has rather been a $Si(OH)_4$-limited system during that time, similar to today (Fig. 4a). During the transition period, when strong upwelling conditions caused intense blooming of *Skeletonema costatum*, utilisation of $Si(OH)_4$ and NO_3^- was very close to a 1:1 ratio. In contrast, the samples from the end of the LIA and especially the recent samples are shifted slightly towards the denitrification curve indicating a higher influence of NO_3^--loss processes. This is particularly the case for the samples from the end of the LIA, which have the lowest $\delta^{30}Si_{opal}$ but at the same time already show a strong increase in $\delta^{15}N_{sed}$ to values of near +6‰. The most likely explanation is that upwelling was strongly increased during those brief periods resulting in high nutrient supply, high productivity, and either more complete NO_3^- utilisation (Gutiérrez et al., 2009) or increased NO_3^--loss caused by enhanced subsurface oxygen depletion. Overall, however, the utilisation signal appears to have dominated both the Si and N isotope records.

If, however, the $\delta^{15}N_{sed}$ is dominated by utilisation it is interesting that in the cores (both B0405-6 and -13) $\delta^{15}N_{sed}$ and proxies for sediment redox conditions (e.g. molybdenum concentrations) are strongly coupled throughout the record (Sifeddine et al., 2008; Gutiérrez

et al., 2009). One direct interpretation could be that the diatom blooms, and subsequently the degradation of the organic matter, strongly control the oxygen availability in the sediments after sedimentation and burial. Therefore, increased diatom productivity and higher $Si(OH)_4$ and NO_3^- utilisation would result in an increase in $\delta^{15}N_{sed}$. At the same time more oxygen is consumed during degradation of the organic matter in the sediments causing more reducing conditions in the sediments. Consequently, a change in the subsurface water column structure, e.g. enhanced re-supply of oxygen via ocean currents, may not be reflected in the $\delta^{15}N_{sed}$ record.

4.1.4 Modelling the Surface Water Utilisation

Following the above considerations we will try to quantify past utilisation based on our data. The theoretical relationship between the degree of surface water nutrient utilisation and the stable isotope composition of Si and N can be described assuming either Rayleigh-type (single input followed by no additional nutrients newly supplied to a particular parcel of water followed by fractional loss as a function of production and export) or steady state (continuous supply and partial consumption of nutrients causing a dynamic equilibrium of the dissolved nutrient concentration and the product) fractionation behaviour (Fig. 5) (Mariotti et al., 1981). The lighter isotopes are preferentially incorporated into the diatom frustules and the organic matter, respectively, leaving the dissolved fraction enriched in the heavier isotopes (Wada and Hattori, 1978; Altabet et al., 1991; De La Rocha et al., 1997). The fractionation between $\delta^{30}Si$ in seawater and $\delta^{30}Si$ in the produced diatom opal has generally been assumed to be -1.1‰ (De La Rocha et al., 1997) whereas between $\delta^{15}N_{NO3-}$ of seawater and $\delta^{15}N$ of the newly formed organic matter it is usually between -3‰ to -6‰ (DeNiro and Epstein, 1981; Minagawa and Wada, 1984). Here we adopted -5‰, which corresponds to present-day conditions along the central Peruvian shelf (Mollier-Vogel et al., 2012).

Along the Peruvian shelf region biological productivity in the euphotic zone is mainly driven by upwelling of nutrients from subsurface waters. For the calculation of the utilisation of these nutrients, an initial $\delta^{30}Si_{Si(OH)4}$ of +1.5‰ (Ehlert et al., 2012) and an initial $\delta^{15}N_{NO3-}$ of +9‰ (Mollier-Vogel et al., 2012) for the upwelled water masses at 14°S is assumed. The lower mean $\delta^{15}N_{sed}$ of about +5‰ and $\delta^{30}Si_{opal}$ of +0.7‰ signatures during the LIA in the southerly core B0405-6 correspond to a dissolved $\delta^{15}N_{NO3-}$ and $\delta^{30}Si_{Si(OH)4}$ isotope signature

of the surface waters of +10‰ and +1.8‰ and a calculated NO_{3^-} and $Si(OH)_4$ utilisation of only 20-30% for steady state-type fractionation (Fig. 5b) and 35-50% for Rayleigh-type fractionation (Fig. 5a) behaviour, respectively. The highest mean values of +1.1‰ for $\delta^{30}Si_{opal}$ and +6.8‰ for $\delta^{15}N_{sed}$ for the transition period correspond to a much higher utilisation of ~60% for steady state-type fractionation and ~80% assuming Rayleigh-type fractionation. Consequently, the calculated utilisation of available $Si(OH)_4$ and NO_3^- more than doubled, whereby bSi concentrations and diatom accumulation rates increased by about a factor of three (Fig. 2e).

The changes in $Si(OH)_4$ and NO_3^- utilisation were of the same order of magnitude and reflect low nutrient utilisation during the LIA and much higher degree of utilisation thereafter. The large increase in $\delta^{15}N_{sed}$ at the end of the LIA has been interpreted to reflect an expansion of nutrient-rich, oxygen-poor subsurface waters (Gutiérrez et al., 2009). However, comparison with $\delta^{30}Si_{opal}$ shows that indeed the increase in $\delta^{15}N_{sed}$ may have occurred as a consequence of the extension of the oxygen minimum zone and increasing subsurface NO_3^--loss but can also be explained by higher surface water utilisation. As Mollier-Vogel et al. (2012) have shown, the subsurface enrichment of $\delta^{15}N_{NO3-}$ caused by NO_3^--loss processes can only be reflected in the sediments under near-complete surface water NO_3^- utilisation, which did obviously not occur at our studied sites.

In the modern samples the $\delta^{30}Si_{opal}$ are characterised by a slight decrease after the transition period from mean value of +1.12‰ to +0.82‰, whereas the $\delta^{15}N_{sed}$ values remain at the same level around +7‰ (Fig. 2). This corresponds to a ~20% higher NO_3^- than $Si(OH)_4$ utilisation (Fig. 5). However, when assuming that diatoms are the dominating primary producers with a NO_3^-:$Si(OH)_4$ uptake ration of ~1, these 20% could be interpreted to reflect the increase in subsurface NO_3^--loss that is not observable during the LIA or the transition period. I.e. during the LIA and the transition period utilisation was the domniating process influencing the $\delta^{15}N_{sed}$ signal, whereas during modern times NO_3^--loss enhanced the signal. By combining the $\delta^{30}Si_{opal}$ and the $\delta^{15}N_{sed}$ records this "additional" signal can be quantified here: if only utilisation would play a role the expected $\delta^{15}N_{sed}$ signal would be ~+6‰ (corresponding to the measured ~+0.8‰ for $\delta^{30}Si_{opal}$, Fig. 5). The additional 1‰ $\delta^{15}N_{sed}$ must be due to NO_3^--loss.

The overall relatively low $\delta^{30}Si_{opal}$ signatures between 0.8‰ and 1.0‰ during the LIA and in the modern part of the records (Figs. 2, 5) document that the utilisation of $Si(OH)_4$ only

changed slightly during the investigated period of time although the accumulation rate of produced diatoms was much higher after the LIA (Fig. 2e) (Gutiérrez et al., 2009). This suggests that the nutrient concentrations in the upwelled subsurface source waters must have been lower during the LIA than they are today. During the LIA large-scale circulation changes, i.e. a weak Walker circulation and a contraction of the SPSH (Conroy et al., 2008; Lamy et al., 2001), caused permanent El Niño-like conditions along the Peruvian upwelling system. During such conditions, the alongshore winds weakened and caused a deepening of the thermo-, oxy- and nutricline, and therefore a reduction of vertical pumping of nutrient-rich and oxygen-depleted subsurface waters off Peru. Such a reduced nutrient supply to the euphotic zone from subsurface waters resulted in an increase in nutrient deficit in surface waters and decreased biological productivity. Enhanced water column oxygenation and lower organic matter flux led to decreased organic matter preservation in the sediments.

4.1.5 Factors Influencing the Reconstruction of the Utilisation Signals

There are two main factors that can influence the reconstruction of nutrient utilisation in the past: 1) a change in the dominating diatom assemblages has to be considered and 2) the interpretation strongly depends on the assumptions for the environmental conditions, e.g. source water signature and isotope enrichment during utilisation.

Varying upwelling and nutrient supply conditions also cause changes in the dominating diatom assemblages. Recent results from culturing experiments suggest species-dependent enrichment factors for diatom-$\delta^{30}Si$ (-0.5‰ to -2.1‰; Sutton et al., 2013) and also diatom frustule-bound $\delta^{15}N$ (-1.9‰ to -11.2‰; Horn et al., 2011). This raises the question whether a change in diatom assemblages may have been the cause for the observed downcore $\delta^{30}Si_{opal}$ and, to a lesser extent, the bulk $\delta^{15}N_{sed}$ variations. The quasi-monospecific diatom layers from the transition period 1820-1870 AD consist mainly of *Skeletonema costatum* (Gutiérrez et al., 2009), for which an enrichment factor ε of -1.0‰ similar to the applied -1.1‰ was determined (De la Rocha et al., 1997). The younger sediments also also contain abundant upwelling-indicative species such as *Thalassionema nitzschioides* and *Chaetoceros sp*. (Abrantes et al., 2007), whereby *Chaetoceros brevis*, a species from the Southern Ocean, has been shown to have a much higher ε of -2.1‰ (Sutton et al., 2013). That means, assuming the same surface water $\delta^{30}Si_{Si(OH)4}$ signatures, a dominance of *Chaetoceros sp*. in the sediments

should result in a lower $\delta^{30}Si_{opal}$ whereas assemblages dominated by *Skeletonema costatum* should be characterised by higher $\delta^{30}Si_{opal}$ signatures, which is exactly what core B0405-6 shows. Consequently, the difference in $\delta^{30}Si_{opal}$ over time could reflect the change in diatom assemblage and not a change in nutrient utilisation. On the other hand, *Chaetoceros brevis* is a polar species and it is not clear whether off Peru it undergoes the same high fractionation factor during frustule growth. It has been shown that the offset between modern surface water $\delta^{30}Si_{Si(OH)4}$ and surface sediment $\delta^{30}Si_{opal}$ along the central Peruvian shelf is between -1.1‰ and -1.3‰ (Ehlert et al., 2012), which indicates that either the enrichment factor for the dominating *Chaetoceros* species off Peru does not deviate significantly from -1.1‰ or that the mixing of different diatoms in the sediment samples overprints any isotopic excursions of single species caused by higher or lower fractionation factors. Given the paucity of data on the fractionation factors for the dominant diatom species off Peru, the importance of the role of downcore changes in the assemblage composition is hard to determine.

The assumed source water $\delta^{30}Si_{Si(OH)4}$ and $\delta^{15}N_{NO3-}$ values of +1.5‰ and +9‰ (Figs. 5, 6), respectively, were measured in the present day subsurface waters under strong upwelling conditions during which high amounts of nutrients are supplied to the euphotic zone (Ehlert et al., 2012; Mollier-Vogel et al., 2012). Under strong upwelling conditions the bottom waters on the shallow shelf are today dominated by the southward directed high-nutrient Peru-Chile Undercurrent (PCUC) (Fig. 1) (Brink et al., 1983). Under LIA-conditions (prevailing El Niño-like conditions), however, atmospheric and oceanic circulation was different; the nutricline was deeper as a consequence of a weak Walker circulation and the winds driving the upwelling were weaker as a consequence of the SPSH contraction (Salvatteci et al. 2014a). In fact, the pumped waters were likely nutrient-depleted, because the Ekman layer did not reach the subsurface nutrient-rich waters. Under these conditions, the subtropical and equatorial nutrient-depleted surface water masses may have occupied the entire surface layer in the coastal realm because they expanded both latitudinally and vertically in the water column (Montes et al., 2011). This may have changed the source water isotopic signatures and would therefore also change the calculated degrees of utilisation. If, for example, the assumed source water $\delta^{15}N_{NO3-}$ was +6‰ instead of +9‰ (e.g. due to weaker subsurface NO_3^- -loss and weaker ^{15}N enrichment during the LIA) the downcore $\delta^{15}N_{sed}$ data of core B0405-6 would all plot closer to the denitrification curve (Fig. 4b). Redox proxies from the records, indeed, indicate a weaker OMZ (Gutiérrez et al., 2009), which would make a lower $\delta^{15}N_{NO3-}$

in source waters likely. However, to date there is no reliable information if and how much the source water $\delta^{30}Si_{Si(OH)4}$ and $\delta^{15}N_{NO3-}$ signatures changed over time.

In the following we thus investigate variations in past water mass circulation, upwelling conditions, as well as material input and transport to reconstruct the source water conditions without considering the potential influence of changes in diatom assemblages.

4.2 Changes in Water Mass Circulation, Detrital Material Input and Transport

The radiogenic isotope composition of the lithogenic particles ($\varepsilon_{Nd\ detritus}$ and $^{87}Sr/^{86}Sr_{detritus}$) of the sediments provides useful information about the source region of material and therefore about changes in material input and transport, either eolian or via ocean currents (e.g. Grousset et al., 1988). Surface sediments along the Peruvian shelf show highly variable signatures, which have overall more radiogenic $\varepsilon_{Nd\ detritus}$ values in the North and much less radiogenic $\varepsilon_{Nd\ detritus}$ values in the South off southern Peru and northern Chile (Ehlert et al., 2013). This north-south trend is a consequence of the southward increasing contributions of material input from the adjacent Andean hinterland rocks. The Andean rocks along the northwestern South American region display a wide range in ε_{Nd} and $^{87}Sr/^{86}Sr$ signatures (Fig. 6) (Sarbas and Nohl, 2009) varying from highly radiogenic ε_{Nd} around 0 and unradiogenic $^{87}Sr/^{86}Sr$ values around 0.704 in the equatorial region in northern Peru to much less radiogenic ε_{Nd} mostly below -4 and more radiogenic $^{87}Sr/^{86}Sr$ mostly above 0.705 in southern Peru and northern Chile. The sedimentary $\varepsilon_{Nd\ detritus}$ and $^{87}Sr/^{86}Sr_{detritus}$ records of the two cores off Callao at 11°S and off Pisco at 14°S show broad similarities, but also some differences. Both cores recorded a significant change in $\varepsilon_{Nd\ detritus}$ and $^{87}Sr/^{86}Sr_{detritus}$, and therefore a change in provenance, at the end of the LIA and during the transition period. Core M771-470, although being located further north, is overall characterised by less radiogenic $\varepsilon_{Nd\ detritus}$ values than core B0405-6 (Figs. 2, 6). The $\varepsilon_{Nd\ detritus}$ of core M771-470 recorded a trend from less radiogenic towards more radiogenic values prior to the end of the LIA, followed by a step of 1.5 ε_{Nd} units towards less radiogenic values, which afterwards remained at that level. In contrast, the $\varepsilon_{Nd\ detritus}$ record of core B0405-6 remained at a level around -3.6 during the LIA and then slightly increased to maximum values of up to -2.5 in the younger part. The $^{87}Sr/^{86}Sr_{detritus}$ record in both cores is mainly characterised by a rapid shift towards more radiogenic values at the end of the LIA, whereby the change was much more pronounced in

555 core M771-470 (Figs. 2d, h). The youngest samples of the cores are in good agreement with
556 measurements of surface sediments from the same area (Figs. 2, 6) (Ehlert et al., 2013). The
557 variability in core M771-470 display the same magnitude as the complete glacial-interglacial
558 variation in core SO147-106KL located at 12°S off Lima (Ehlert et al., 2013). All data of both
559 M771-470 and B0405-6 plot within the provenance fields of southern Peru and northern Chile
560 (Fig. 6).

561 Today, material input along the Peruvian shelf occurs mostly via riverine and minor eolian
562 input (Molina-Cruz, 1977; Scheidegger and Krissek, 1982). The LIA, however, was
563 characterised by wetter conditions (Haug et al., 2001; Gutiérrez et al., 2009). These changes
564 in precipitation were associated with the position of the ITCZ, changes in Walker ciculation,
565 and expansion/contraction of the South Pacific Subtropical High (SPSH) (Salvatteci et al.,
566 2014a). Additionally, there has been a tight connection to northern hemisphere climate.
567 Speleothem records from the central Peruvian Andes for example indicate a pronounced link
568 to North Atlantic climate (Kanner et al., 2013). During cold periods like the LIA, the Peruvian
569 upwelling region exhibited an El Niño-like mean state (Salvatteci et al., 2014a) due to the
570 mean southward migration of the ITCZ and the associated precipitation belt, which also
571 caused more intense rainfall in the central Andean hinterland (Rabatel et al., 2008; Reuter et
572 al., 2009). Most terrigenous particles and weathering products such as clay minerals from the
573 LIA show indications of increased riverine transport and discharge (Sifeddine et al., 2008;
574 Salvatteci et al., 2014a). Consequently, material input during the LIA was dominated by local
575 sources due to the higher river discharge.

576 After the end of the LIA the region experienced a northward displacement of the ITCZ and
577 the northern rim of the SPSH to their modern position, coupled with an enhancement of the
578 atmospheric Walker circulation (Gutiérrez et al., 2009). The climate in the EEP became drier
579 and alongshore winds became stronger, riverine input diminished and eolian dust input
580 increased. The wind-blown dust has mainly originated from the Atacama Desert located in the
581 southern Peruvian and northern Chilean Andes (Molina-Cruz, 1977). This material has less
582 radiogenic ε_{Nd} and much more radiogenic $^{87}Sr/^{86}Sr$ values (Fig. 6) (Sarbas and Nohl, 2009).
583 The record of core M771-470 is in agreement with this. The LIA-sediments indicate a local
584 origin, probably via riverine input, whereas the younger sediments display characteristics
585 from a more southerly origin and therefore increased eolian sources, possibly from the
586 Atacama Desert. The signatures and overall small variations in core B0405-6 are much more

difficult to interpret. There are fewer rivers in Southern Peru around Pisco compared to the Callao region. Therefore, riverine-derived material from northern and central Peru, which is transported via the PCUC, can get dispersed further south and can be deposited in the Pisco region. On the other hand, the influence of eolian deposition should be much higher at the southern core location. During the LIA river input increased in southern Peru as well, whereas eolian deposition was low. The invariate signature observed might be the result of mixing of sediment from the different sources. Also, in comparison to core M771-470 core B0405-6 is located much closer to the coast, which most likely diminished the differences in material input and transport between the LIA- and modern conditions.

In summary, our combined proxy information coherently hints to the same controlling processes that we already identified on glacial-interglacial timescales (Ehlert et al., 2013) and to different ENSO pattern during the LIA (enhanced El Niño-like conditions) and in modern times (La-Nina-like conditions). The locally sourced radiogenic isotope signatures show that during the LIA precipitation and runoff from the hinterland was higher but this could not compensate for the lower nutrient supply via diminished upwelling. Eolian wind forcing was low and the source waters of the upwelling carried less nutrients. Consequently, diatom productivity and nutrient utilisation were low. In contrast, after the end of the LIA radiogenic isotopes indicate diminished river runoff and increased dust transport, which is in agreement with an overall drier climate, probably driven by an expansion of the SPSH, and a shoaling of the thermocline/nutricline due to a stronger atmospheric Walker circulation. Especially in more recent times, the efficient remineralisation of nutrients from subsurface waters fuelled enhanced diatom productivity most liekly responsible for higher nutrient utilisation in surface waters as well as enhanced oxygen demand and NO_3^--loss in subsurface waters.

5 Conclusions

Proxies of productivity, nutrient utilisation and material provenance (bSi and N content, $\delta^{30}Si_{opal}$, $\delta^{15}N_{sed}$, $\varepsilon_{Nd\ detritus}$, and $^{87}Sr/^{86}Sr_{detritus}$) from two cores from the Peruvian shelf recorded significant changes in surface water $Si(OH)_4$ and NO_3^- concentration and utilisation due to changes in upwelling intensity and nutrient supply. During the LIA the overall nutrient content in the water column and in surface waters was low because the upwelling source waters contained less nutrients. Consequently, the Peruvian upwelling regime was

618 characterised by persistently reduced primary productivity. The reasons for this were most
619 likely a contraction of the South Pacific Subtropical High and a weaker Walker circulation
620 that resulted in a weakening of alongshore winds and a deepening of the nutricline.

621 The enhanced rainfall associated with higher moisture on land during prevailing El Niño-like
622 conditions during the LIA were recorded by the radiogenic isotope composition of the detrital
623 material along the shelf, which was mainly transported via rivers from the Andean hinterland.
624 At the end of the LIA, in accordance with a northward shift of the ITCZ and an intensification
625 of wind strength a higher dust transport of particles associated with drier conditions and
626 eolian forcing is reflected by the radiogenic isotope composition of the detrital sediments.
627 These conditions were also reflected in increasing upwelling strength, a rapid shoaling of the
628 thermocline and nutricline, as well as enhanced nutrient supply and productivity to the surface
629 waters. During a transition period a marked increase in diatom blooming events doubled the
630 $Si(OH)_4$ and NO_3^- utilisation compared to the LIA, and was also higher than present day
631 utilisation. After that transition period more persistent non-El Niño conditions favoured a high
632 productivity accompanied by moderate utilisation of nutrients. Utilisation was similar to the
633 LIA but productivity was much higher, which reflects the much higher concentrations of
634 nutrients in surface waters.

635 Most studies of past coastal upwelling regions have argued so far that the sedimentary $\delta^{15}N_{sed}$
636 records were dominated by the large N isotope fractionation signature occurring during NO_3^--
637 loss processes (denitrification or anammox) in oxygen-depleted subsurface waters upwelling.
638 Comparison between $\delta^{30}Si_{opal}$ and $\delta^{15}N_{sed}$ in the same sediment samples of our study and
639 assuming similar source water signatures as today, however, indicate that except for the
640 period of time since ~1870 AD, the $\delta^{15}N_{sed}$ signatures to a large extent reflect expected
641 utilisation signals, which has important implications for the reconstruction of variations in the
642 intensity of oxygen depletion, the N cycle of the past and its controlling factors.

643

644 **Acknowledgements**

645 This work is a contribution of Sonderforschungsbereich 754 "Climate -
646 Biogeochemistry Interactions in the Tropical Ocean" (www.sfb754.de), which is supported by
647 the Deutsche Forschungsgemeinschaft. We acknowledge the help of Jutta Heinze in the
648 laboratory of GEOMAR for the biogenic opal concentration measurements. We thank Ulrike

649 Lomnitz and Klaus Wallmann for their help with the ^{210}Pb dating and the establishment of the
650 age model of core M771-470.

651

652 **References**

653 Abrantes, F., Lopes, C., Mix, A. C., and Pisias, N. G.: Diatoms in Southeast Pacific surface
654 sediments reflect environmental properties, Quaternary Science Reviews, 26, 155–169, 2007.
655 doi:10.1016/j.quascirev.2006.02.022

656 Agnihotri, R., Altabet, M. A., Herbert, T. D., and Tierney, J. E.: Subdecadally resolved
657 paleoceanography of the Peru margin during the last two millennia, Geochemistry
658 Geophysics Geosystems, 9(Q05013), 2008. doi:10.1029/2007GC001744

659 Albarède, F., Telouk, P., Blichert-Toft, J., Boyet, M., Agranier, A., and Nelson, B.: Precise
660 and accurate isotopic measurements using multiple-collector ICPMS, Geochimica et
661 Cosmochimica Acta, 68(12), 2725–2744, 2004. doi:10.1016/j.gca.2003.11.024

662 Altabet, M. A., Deuser, W. G., Honjo, S., and Stienen, C.: Seasonal and depth-related changes
663 in the source of sinking particles in the North Atlantic, Nature, 354, 136–139, 1991.

664 Altabet, M. A., and Francois, R.: Sedimentary nitrogen isotopic ratio as a recorder for surface
665 ocean nitrate utilisation, Global Biogeochemical Cycles, 8(1), 103–116, 1994.

666 Altabet, M. A., Pilskaln, C., Thunell, R. C., Pride, C. J., Sigman, D. M., Chavez, F. P., and
667 Francois, R.: The nitrogen isotope biogeochemistry of sinking particles from the margin of
668 the Eastern North Pacific, Deep-Sea Research I, 46, 655–679, 1999.

669 Altabet, M. A., Ryabenko, E., Stramma, L., Wallace, D. W. R., Frank, M., Grasse, P., and
670 Lavik, G.: An eddy-stimulated hotspot for fixed nitrogen-loss from the Peru oxygen minimum
671 zone, Biogeosciences, 9(12), 4897–4908, 2012. doi:10.5194/bg-9-4897-2012

672 Bird, B. W., Abbott, M. B., Vuille, M., Rodbell, D. T., Stansell, N. D., and Rosenmeier, M.
673 F.: A 2,300-year-long annually resolved record of the South American summer monsoon
674 from the Peruvian Andes, PNAS, 108(21), 8583–8588, 2011. doi:10.1073/pnas.1003719108

675 Brink, K. H., Halpern, D., Huyer, A., and Smith, R. L.: The Physical Environment of the
676 Peruvian Upwelling System, Progress in Oceanography, 12, 285–305, 1983.

677 Bruland, K. W., Rue, E. L., Smith, G. J., and DiTullio, G. R.: Iron, macronutrients and diatom
678 blooms in the Peru upwelling regime: brown and blue waters of Peru, Marine Chemistry, 93,
679 81–103, 2005. doi:10.1016/j.marchem.2004.06.011

680 Brzezinski, M. A.: The Si:C:N ratio of marine diatoms: interspecific variability and the effect
681 of some environmental variables, Journal of Phycology, 21(3), 347–357, 1985.

682 Brzezinski, M. A., Pride, C. J., Franck, V. M., Sigman, D. M., Sarmiento, J. L., Matsumoto,
683 K., Gruber, N., Rau, G. H., and Coale, K. H.: A switch from Si(OH)4 to NO3- depletion in
684 the glacial Southern Ocean, Geophysical Research Letters, 29(12), 3–6, 2002.
685 doi:10.1029/2001GL014349

686 Codispoti, L. A., Brandes, J. A., Christensen, J. P., Devol, A. H., Naqvi, S. W. A., Paerl, H.
687 W., and Yoshinary, T.: The oceanic fixed nitrogen and nitrous oxide budgets: Moving targets
688 as we enter the anthropocene? Scientia Marina, 65, 85–105, 2001.

689 Cohen, A. S., O'Nions, R. K., Siegenthaler, R., and Griffin, W. L.: Chronology of the
690 pressure-temperature history recorded by a granulite terrain, Contributions to Mineralogy and
691 Petrology, 98, 303–311, 1988.

692 Conroy, J. L., Restrepo, A., Overpeck, J. T., Steinitz-Kannan, M., Cole, J. E., Bush, M. B.,
693 and Colinvaux, P. A.: Unprecedented recent warming of surface temperatures in the eastern
694 tropical Pacific Ocean, Nature Geoscience, 2, 46–50, 2008. doi:10.1038/ngeo390

695 Dalsgaard, T., Canfield, D. E., Petersen, J., Thamdrup, B., and Acuna-González, J.: N2
696 production by the anammox reaction in the anoxic water column of Golfo Dulce, Costa Rica,
697 Nature, 422, 606–608, 2003.

698 De La Rocha, C. L., Brzezinski, M. A., and DeNiro, M. J.: Fractionation of silicon isotopes
699 by marine diatoms during biogenic silica formation, Geochimica et Cosmochimica Acta,
700 61(23), 5051–5056, 1997.

De La Rocha, C. L., Brzezinski, M. A., DeNiro, M. J., and Shemesh, A.: Silicon-isotope composition of diatoms as an indicator of past oceanic changes, Nature, 395, 680–683, 1998.

De Pol-Holz, R., Robinson, R. S., Hebbeln, D., Sigman, D. M., and Ulloa, O.: Controls on sedimentary nitrogen isotopes along the Chile margin, Deep-Sea Research II, 56, 1042–1054, 2009. doi:10.1016/j.dsr2.2008.09.014

De Pol-Holz, R., Ulloa, O., Dezileau, L., Kaiser, J., Lamy, F., and Hebbeln, D.: Melting of the Patagonian Ice Sheet and deglacial perturbations of the nitrogen cycle in the eastern South Pacific, Geophysical Research Letters, 33(L04704), 2006. doi:10.1029/2005GL024477

De Pol-Holz, R., Ulloa, O., Lamy, F., Dezileau, L., Sabatier, P., and Hebbeln, D.: Late Quaternary variability of sedimentary nitrogen isotopes in the eastern South Pacific Ocean, Paleoceanography, 22(PA2207), 2007. doi:10.1029/2006PA001308

De Souza, G. F., Reynolds, B. C., Rickli, J., Frank, M., Saito, M. A., Gerringa, L. J. A., and Bourdon, B.: Southern Ocean control of silicon stable isotope distribution in the deep Atlantic Ocean, Global Biogeochemical Cycles, 26(GB2035), 2012. doi:10.1029/2011GB004141

DeMaster, D. J.: The supply and accumulation of silica in the marine environment, Geochimica et Cosmochimica Acta, 45, 1715–1732, 1981.

DeNiro, M. J., and Epstein, S.: Influence of diet on the distribution of nitrogen isotopes in animals, Geochimica et Cosmochimica Acta, 45(3), 341–351, 1981.

Díaz-Ochoa, J. A., Lange, C. B., Pantoja, S., De Lange, G. J., Gutiérrez, D., Munoz, P., and Salamanca, M.: Fish scales in sediments from off Callao, central Peru, Deep-Sea Research II, 56, 1113–1124, 2009. doi:10.1016/j.dsr2.2008.09.015

Díaz-Ochoa, J. A., Pantoja, S., De Lange, G. J., Lange, C. B., Sánchez, G. E., Acuña, V. R., Muñoz, P., and Vargas, G.: Oxygenation variability in Mejillones Bay, off northern Chile, during the last two centuries, Biogeosciences, 8(1), 137–146, 2011. doi:10.5194/bg-8-137-2011

726 Egan, K. E., Rickaby, R. E. M., Leng, M. J., Hendry, K. R., Sloane, H. J., Bostock, H. C., and
727 Halliday, A. N.: Diatom silicon isotopes as a proxy for silicic acid utilisation: A Southern
728 Ocean core top calibration, Geochimica et Cosmochimica Acta, 96, 174–192, 2012.
729 doi:10.1016/j.gca.2012.08.002

730 Ehlert, C., Grasse, P., Mollier-Vogel, E., Böschen, T., Franz, J., De Souza, G. F., Reynolds,
731 B. C., Stramma, L., and Frank, M.: Factors controlling the silicon isotope distribution in
732 waters and surface sediments of the Peruvian coastal upwelling, Geochimica et
733 Cosmochimica Acta, 99, 128–145, 2012. doi:10.1016/j.gca.2012.09.038

734 Ehlert, C., Grasse, P., and Frank, M.: Changes in silicate utilisation and upwelling intensity
735 off Peru since the Last Glacial Maximum - insights from silicon and neodymium isotopes,
736 Quaternary Science Reviews, 72, 18–35, 2013. doi:10.1016/j.quascirev.2013.04.013

737 Estrada, M., and Blasco, D.: Phytoplankton assemblages in coastal upwelling areas, In: C.
738 Bas, R. Margalef, and P. Rubies (Eds.), Simposio Internacional Sobre Las Areas de
739 Afloramiento Mas Importantes del Oeste Africano (Cabo Blanco y Benguela), Barcelona:
740 Instituto de Investigaciones Pesqueras, 379–402. 1985.

741 Georg, R. B., Reynolds, B. C., Frank, M., and Halliday, A. N.: New sample preparation
742 techniques for the determination of Si isotopic compositions using MC-ICPMS, Chemical
743 Geology, 235, 95–104, 2006. doi:10.1016/j.chemgeo.2006.06.006

744 Goldstein, S. L., O'Nions, R. K., & Hamilton, P. J.: A Sm - N d isotopic study of atmospheric
745 dusts and particulates from major river systems, Earth and Planetary Science Letters, 70(2),
746 221–236, 1984.

747 Grasse, P., Stichel, T., Stumpf, R., Stramma, L., and Frank, M.: The distribution of
748 neodymium isotopes and concentrations in the Eastern Equatorial Pacific: Water mass
749 advection versus particle exchange, Earth and Planetary Science Letters, 353-354, 198–207,
750 2012. doi:10.1016/j.epsl.2012.07.044

751 Grasse, P., Ehlert, C., and Frank, M.: The Influence of Water Mass Mixing on the Dissolved
752 Si Isotope Composition in the Eastern Equatorial Pacific, Earth and Planetary Science Letters,
753 380, 60–71, 2013. doi:10.1016/j.epsl.2013.07.033

754 Grousset, F. E., Biscaye, P. E., Zindler, A., Prospero, J., and Chester, R.: Neodymium
755 isotopes as tracers in marine sediments and aerosols: North Atlantic, Earth and Planetary
756 Science Letters, 87, 367–378, 1988.

757 Grove, M. J.: The initiation of the "Little Ice Age" in regions round the North Atlantic,
758 Climatic Change, 48, 53–82, 2001.

759 Gutiérrez, D., Sifeddine, A., Field, D. B., Ortlieb, L., Vargas, G., Chavez, F. P., Velazco, F.,
760 Ferreira-Bartrina, V., Tapia, P. M., Salvatteci, R., Boucher, H., Morales, M. C., Valdés, J.,
761 Reyss, J.-L., Campusano, A., Boussafir, M., Mandeng-Yogo, M., García, M., and
762 Baumgartner, T.: Rapid reorganization in ocean biogeochemistry off Peru towards the end of
763 the Little Ice Age, Biogeosciences, 6, 835–848, 2009.

764 Gutiérrez, D., Sifeddine, A., Reyss, J.-L., Vargas, G., Velazco, F., Salvatteci, R., Ferreira-
765 Bartrina, V., Ortlieb, L., Field, D. B., Baumgartner, T., Boussafir, M., Boucher, H., Valdés, J.,
766 Marinovic, L., Soler, P., and Tapia, P. M.: Anoxic sediments off Central Peru record
767 interannual to multidecadal changes of climate and upwelling ecosystem during the last two
768 centuries, Advances in Geosciences, 6, 119–125, 2006.

769 Horn, M. G., Robinson, R. S., Rynearson, T. A., and Sigman, D. M.: Nitrogen isotopic
770 relationship between diatom-bound and bulk organic matter of cultured polar diatoms,
771 Paleoceanography, 26(PA3208), 2011. doi:10.1029/2010PA002080

772 Horwitz, E. P., Chiarizia, R., and Dietz, M. L.: A Novel Strontium-Selective Extraction
773 Chromatographic Resin, Solvent Extraction and Ion Exchange, 10(2), 313–336, 1992.
774 doi:10.1080/07366299208918107

775 Hutchins, D. A., Hare, C. E., Weaver, R. S., Zhang, Y., Firme, G. F., DiTullio, G. R., Alm,
776 M. B., Riseman, S. F., Maucher, J. M., Geesey, M. E., Trick, C. G., Smith, G. J., Rue, E. L.,
777 Conn, J., and Bruland, K. W.: Phytoplankton iron limitation in the Humboldt Current and
778 Peru Upwelling, Limnology and Oceanography, 47(4), 997–1011, 2002.

779 Kanner, L. C., Burns, S. J., Cheng, H., Edwards, R. L., and Vuille, M.: High-resolution
780 variability of the South American summer monsoon over the last seven millennia: insights

781 from a speleothem record from the central Peruvian Andes. Quaternary Science Reviews, 75,
782 1–10, 2013. doi:10.1016/j.quascirev.2013.05.008

783 Kessler, W. S.: The circulation of the eastern tropical Pacific: A review, Progress in
784 Oceanography, 69, 181–217, 2006. doi:10.1016/j.pocean.2006.03.009

785 Lacan, F., and Jeandel, C.: Tracing Papua New Guinea imprint on the central Equatorial
786 Pacific Ocean using neodymium isotopic compositions and Rare Earth Element patterns,
787 Earth and Planetary Science Letters, 186, 497–512, 2001.

788 Lam, P., Lavik, G., Jensen, M. M., Van de Vossenberg, J., Schmid, M., Woebken, D.,
789 Gutiérrez, D., Amann, R., Jetten, M. S. M., and Kuypers, M. M. M.: Revising the nitrogen
790 cycle in the Peruvian oxygen minimum zone, PNAS, 106(12), 4752–4757, 2009.

791 Lamb, H. H.: The early Medieval Warm Epoch and its sequel, Palaeogeography,
792 Palaeoclimatology, Palaeoecology, 1, 13–37, 1965.

793 Lamy, F., Hebbeln, D., Röhl, U., and Wefer, G.: Holocene rainfall variability in southern
794 Chile: a marine record of latitudinal shifts of the Southern Westerlies. Earth and Planetary
795 Science Letters, 185, 369–382, 2001.

796 Liu, K.-K., and Kaplan, I. R.: The eastern tropical Pacific as a source of 15N-enriched nitrate
797 in seawater off southern Califomia. Limnology and Oceanography, 34(5), 820–830, 1989.

798 Mariotti, A., Germon, J. C., Hubert, P., Kaiser, P., Letolle, R., Tardieux, A., and Tardieux, P.:
799 Experimental determination of nitrogen kinetic isotope fractionation: some principles;
800 illustration for the denitrification and nitrification processes, Plant and Soil, 62, 413–430,
801 1981.

802 Meysman, F. J. R., Boudreau, B. P., and Middelburg, J. J.: Modeling reactive transport in
803 sediments subject to bioturbation and compaction, Geochimica et Cosmochimica Acta,
804 69(14), 3601–3617, 2005. doi:10.1016/j.gca.2005.01.004

805 Minagawa, M., and Wada, E.: Stepwise enrichment of 15N along food chains: Further
806 evidence and the relation between d15N and animal age, Geochimica et Cosmochimica Acta,
807 48(5), 1135–1140, 1984.

808 Molina-Cruz, A.: The Relation of the Southern Trade Winds to Upwelling Processes during
809 the Last 75,000 Years, Quaternary Research, 8, 324–338, 1977.

810 Mollier-Vogel, E., Ryabenko, E., Martinez, P., Wallace, D. W. R., Altabet, M. A., and
811 Schneider, R. R.: Nitrogen isotope gradients off Peru and Ecuador related to upwelling,
812 productivity, nutrient uptake and oxygen deficiency, Deep-Sea Research I, 70, 14–25, 2012.
813 doi:10.1016/j.dsr.2012.06.003

814 Montes, I., Schneider, W., Colas, F., Blanke, B., and Echevin, V.: Subsurface connections in
815 the eastern tropical Pacific during La Niña 1999 – 2001 and El Niño 2002 – 2003, Journal of
816 Geophysical Research, 116(C12022), 2011. doi:10.1029/2011JC007624

817 Morley, D. W., Leng, M. J., Mackay, A. W., Sloane, H. J., Rioual, P., and Battarbee, R. W.:
818 Cleaning of lake sediment samples for diatom oxygen isotope analysis, Journal of
819 Paleilimnology, 31, 391–401, 2004.

820 Müller, P. J., and Schneider, R. R.: An automated leaching method for the determination of
821 opal in sediments and particulate matter, Deep-Sea Research I, 40(3), 425–444, 1993.

822 Piepgras, D. J., and Wasserburg, G. J.: Isotopic Composition of Neodymium in Waters from
823 the Drake Passage, Science, 217, 207–214, 1982.

824 Rabatel, A., Francou, B., Jomelli, V., Naveau, P., and Grancher, D.: A chronology of the
825 Little Ice Age in the tropical Andes of Bolivia (16°S) and its implications for climate
826 reconstruction, Quaternary Research, 70(2), 198–212, 2008. doi:10.1016/j.yqres.2008.02.012

827 Reuter, J., Stott, L., Khider, D., Sinha, A., Cheng, H., and Edwards, R. L.: A new perspective
828 on the hydroclimate variability in northern South America during the Little Ice Age,
829 Geophysical Research Letters, 36(L21706), 2009. doi:10.1029/2009GL041051

Reynolds, B. C., Aggarwal, J., André, L., Baxter, D. C., Beucher, C. P., Brzezinski, M. A., Engström, E., Georg, R. B., Land, M., Leng, M. J., Opfergelt, S., Rodushkin, I., Sloane, H. J., Van den Boorn, S. H. J. M., Vroon, P. Z., and Cardinal, D.: An inter-laboratory comparison of Si isotope reference materials, Journal of Analytical Atomic Spectrometry, 22(5), 561, 2007. doi:10.1039/b616755a

Reynolds, B. C., Frank, M., and Halliday, A. N.: Evidence for a major change in silicon cycling in the subarctic North Pacific at 2.73 Ma, Paleoceanography, 23(PA4219), 2008. doi:10.1029/2007PA001563

Sachs, J. P., Sachse, D., Smittenberg, R. H., Zhang, Z., Battisti, D. S., and Golubic, S.: Southward movement of the Pacific intertropical convergence zone AD 1400-1850, Nature Geoscience, 2, 519–525, 2009. doi:10.1038/NGEO554

Salvatteci, R., Gutiérrez, D., Field, D. B., Sifeddine, A., Ortlieb, L., Bouloubassi, I., Boussafir, M., Boucher, H., and Cetin, F.: The response of the Peruvian Upwelling Ecosystem to centennial-scale global change during the last two millennia, Climate of the Past, 10(2), 715-731, 2014a. doi: 10.5194/cp-10-715-2014

Salvatteci, R., Field, D. B., Sifeddine, A., Ortlieb, L., Ferreira-Bartrina, V., Baumgartner, T., Caquineau, S., Velazco, F., Reyss, J.-L., Sanchez-Cabeza, J. A., and Gutiérrez, D.: Cross-stratigraphies from a seismically active mud lens off Peru indicate horizontal extensions of laminae, missing sequences, and a need for multiple cores for high resolution records, Marine Geology, 357, 72-89, 2014b. doi: 10.1016/j.margeo.2014.07.008

Sarbas, B., and Nohl, U.: The GEOROC database – A decade of “online geochemistry”, Geochimica et Cosmochimica Acta, (Goldschmidt Abstracts), A1158, 2009.

Scheidegger, K. F., and Krissek, L. A.: Dispersal and deposition of eolian and fluvial sediments off Peru and northern Chile, Geological Society of America Bulletin, 93(2), 150–162, 1982. doi:10.1130/0016-7606(1982)93<150

Sifeddine, A., Gutiérrez, D., Ortlieb, L., Boucher, H., Velazco, F., Field, D. B., Vargas, G., Boussafir, M., Salvatteci, R., Ferreira-Bartrina, V., García, M., Valdés, J., Caquineau, S., Mandeng-Yogo, M., Cetin, F., Solis, J., Soler, P., and Baumgartner, T.: Laminated sediments

858 from the central Peruvian continental slope: A 500 year record of upwelling system
859 productivity, terrestrial runoff and redox conditions, Progress in Oceanography, 79, 190–197,
860 2008. doi:10.1016/j.pocean.2008.10.024

861 Sutton, J. N., Varela, D. E., Brzezinski, M. A., and Beucher, C. P.: Species-dependent silicon
862 isotope fractionation by marine diatoms, Geochimica et Cosmochimica Acta, 104, 300–309,
863 2013. doi:10.1016/j.gca.2012.10.057

864 Takeda, S.: Influence of iron availability on nutrient consumption ratio of diatoms in oceanic
865 waters, Nature, 393, 774–777, 1998.

866 Tanaka, T., Togashi, S., Kamioka, H., Amakawa, H., Kagami, H., Hamamoto, T., Yuhara,
867 M., Orihashi, Y., Yoneda, S., Shimizu, H., Kunimaru, T., Takahashi, K., Yanagi, T., Nakano,
868 T., Fujimaki, H., Shinjo, R., Asahara, Y., Tanimizu, M., and Dragusanu, C.: JNdi-1: a
869 neodymium isotopic reference in consistency with LaJolla neodymium, Chemical Geology,
870 168, 279–281, 2000.

871 Unkel, I., Kadereit, A., Mächtle, B., Eitel, B., Kromer, B., Wagner, G., and Wackler, L.:
872 Dating methods and geomorphic evidence of palaeoenvironmental changes at the eastern
873 margin of the South Peruvian coastal desert (14°30'S) before and during the Little Ice Age,
874 Quaternary International, 175, 3–28, 2007. doi:10.1016/j.quaint.2007.03.006

875 Valdés, J., Ortlieb, L., Gutiérrez, D., Marinovic, L., Vargas, G., and Sifeddine, A.: 250 years
876 of sardine and anchovy scale deposition record in Mejillones Bay, northern Chile, Progress in
877 Oceanography, 79(2-4), 198–207, 2008. doi:10.1016/j.pocean.2008.10.002

878 Vargas, G., Pantoja, S., Rutllant, J. A., Lange, C. B., and Ortlieb, L.: Enhancement of coastal
879 upwelling and interdecadal ENSO-like variability in the Peru-Chile Current since late 19th
880 century, Geophysical Research Letters, 34(L13607), 2007. doi:10.1029/2006GL028812

881 Vuille, M., Francou, B., Wagnon, P., Juen, I., Kaser, G., Mark, B. G., and Bradley, R. S.:
882 Climate change and tropical Andean glaciers: Past, present and future, Earth-Science
883 Reviews, 89, 79–96, 2008. doi:10.1016/j.earscirev.2008.04.002

884 Wada, E., and Hattori, A.: Nitrogen isotope effects in the assimilation of inorganic
885 nitrogenous compounds by marine diatoms, Geomicrobiology Journal, 1(1), 85–101, 1978.
886 doi:10.1080/01490457809377725

887

888 Table 1. Downcore records of core M77/1-470 for $\delta^{30}Si_{opal}$ (‰), bSi content (wt%) and
889 $^{143}Nd/^{144}Nd$, ε_{Nd} and $^{87}Sr/^{86}Sr$ of detrital material. $2\sigma_{(sd)}$ represents the external
890 reproducibilities of repeated sample (Si) and standard (Nd, Sr) measurements.

depth (cm)	$\delta^{30}Si_{opal}$ (‰)	$2\sigma_{(sd)}$	bSi (wt%)	$^{143}Nd/^{144}Nd_{detritus}$	$\varepsilon_{Nd\ detritus}$	$2\sigma_{(sd)}$	$^{87}Sr/^{86}Sr_{detritus}$	$2\sigma_{(sd)}$
0.5	1.03	0.15	18.8	-	-	-	-	-
1.5	-	-	18.6	-	-	-	-	-
2.5	-	-	22.2	-	-	-	-	-
3.5	0.93	0.08	16.9	0.512369	-5.2	0.3	0.709315	1.5E-05
4.5	-	-	16.3	-	-	-	-	-
5.5	-	-	17.2	0.512381	-5.0	0.3	0.709356	1.5E-05
7	-	-	19.5	-	-	-	-	-
9	0.96	0.09	19.8	0.512398	-4.7	0.3	0.708822	1.5E-05
11	-	-	18.8	-	-	-	-	-
13	-	-	15.9	-	-	-	-	-
15	-	-	-	0.512383	-5.0	0.3	0.708737	1.5E-05
16	0.96	0.07	19.3	-	-	-	-	-
19	-	-	-	0.512386	-4.9	0.3	0.708552	1.5E-05
20	1.05	0.10	18.9	0.512410	-4.5	0.3	0.708412	8.0E-06
23	-	-	-	0.512393	-4.8	0.3	0.708720	1.5E-05
24	1.15	0.13	26.9	-	-	-	-	-
26	-	-	-	0.512387	-4.9	0.3	0.707482	8.0E-06
27	-	-	-	0.512397	-4.7	0.3	0.707555	1.5E-05
28	1.00	0.14	14.0	-	-	-	-	-
29	-	-	-	0.512452	-3.6	0.3	0.706549	1.5E-05
32	0.55	0.17	10.1	0.512442	-3.8	0.3	0.706763	1.5E-05
32	-	-	-	0.512445	-3.8	0.3	0.706469	8.0E-06
36	1.10	0.15	14.4	0.512419	-4.3	0.3	0.706767	8.0E-06
40	0.79	0.11	12.3	0.512408	-4.5	0.3	0.706964	8.0E-06
44	0.91	0.18	15.0	0.512421	-4.2	0.3	0.707057	8.0E-06
48	0.75	0.05	-	0.512395	-4.7	0.3	0.707816	8.0E-06

891
892

893 Table 2. Downcore records of core B0405-6 for $\delta^{30}Si_{opal}$ (‰), $bSiO_2$ content (wt%) and
894 $^{143}Nd/^{144}Nd$, ε_{Nd} and $^{87}Sr/^{86}Sr$ of detrital material. $2\sigma_{(sd)}$ represents the external
895 reproducibilities of repeated sample (Si) and standard (Nd, Sr) measurements.

year AD	$\delta^{30}Si_{opal}$ (‰)	$2\sigma_{(sd)}$	bSi (wt%)	$^{143}Nd/^{144}Nd_{detritus}$	$\varepsilon_{Nd\ detritus}$	$2\sigma_{(sd)}$	$^{87}Sr/^{86}Sr_{detritus}$	$2\sigma_{(sd)}$
1950	0.91	0.15	21.7	0.512507	-2.6	0.1	0.708372	8.0E-06
1925	0.83	0.15	21.0	0.512460	-3.5	0.3	0.707923	8.0E-06
1903	0.62	0.10	18.9	0.512487	-2.9	0.3	0.707715	8.0E-06
1857	1.02	0.16	34.4	0.512471	-3.3	0.3	0.707829	8.0E-06
1857	1.22	0.14	37.7	0.512481	-3.1	0.1	0.707736	8.0E-06
1818	0.56	0.15	12.6	0.512468	-3.3	0.3	0.707702	8.0E-06
1793	0.82	0.14	15.8	0.512446	-3.7	0.3	0.707265	8.0E-06
1761	0.71	0.16	13.5	0.512627	-0.2	0.3	0.707296	8.0E-06
1698	0.73	0.09	17.3	0.512462	-3.4	0.3	0.707278	8.0E-06
1564	0.81	0.12	20.8	0.512467	-3.3	0.3	0.707281	8.0E-06
1475	0.77	0.04	17.1	0.512427	-4.1	0.3	0.707959	8.0E-06
1370	0.80	0.23	34.2	0.512509	-2.5	0.3	0.707111	8.0E-06

896

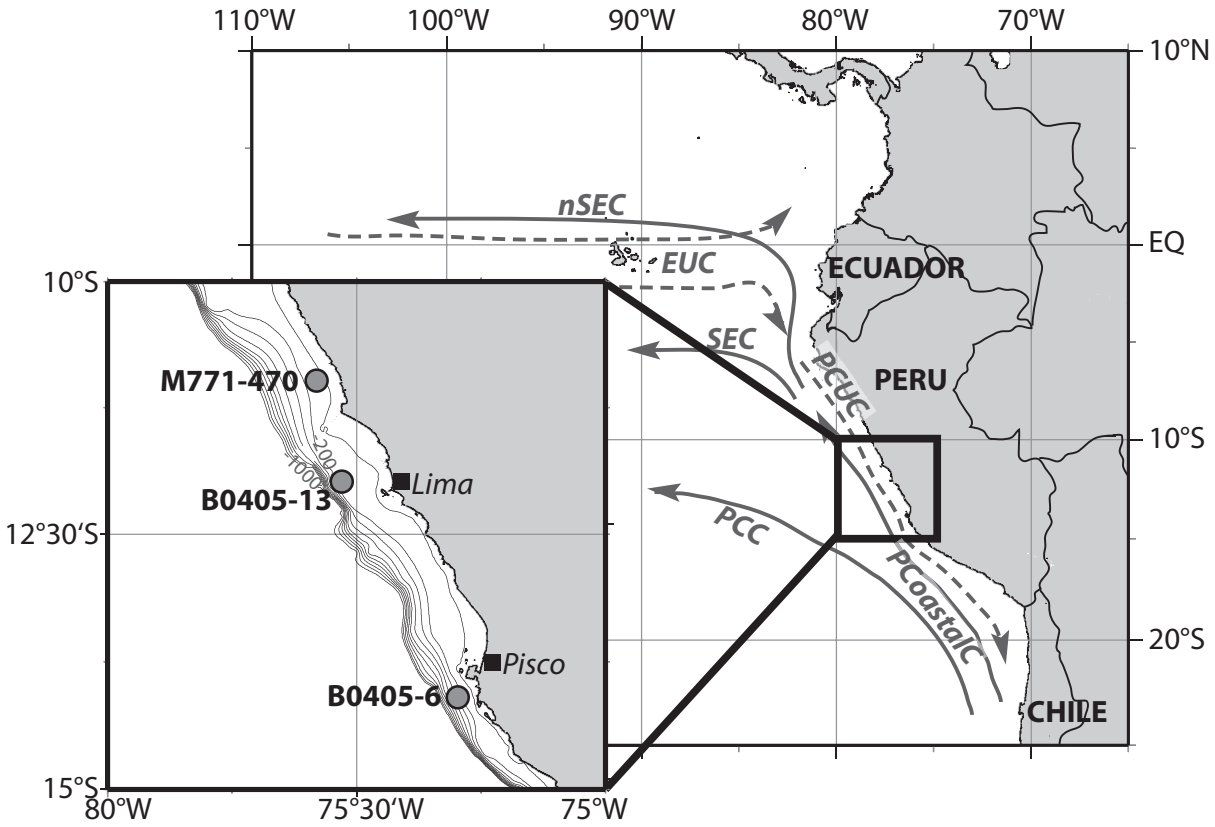

Figure 1. Schematic circulation patterns in the Eastern Equatorial Pacific. Surface currents (solid lines): (n)SEC: (northern) South Equatorial Current, PCC: Peru-Chile Current, PCoastalC: Peru Coastal Current; subsurface currents (dashed lines): EUC Equatorial Undercurrent, PCUC Peru-Chile Undercurrent (after Brink, 1983; Kessler, 2006), the inset shows the detailed location of cores M771-470, B0405-6 and B0405-13 (grey dots). The bathymetry is given for 0 to 1000 m water depth in 100 m increments.

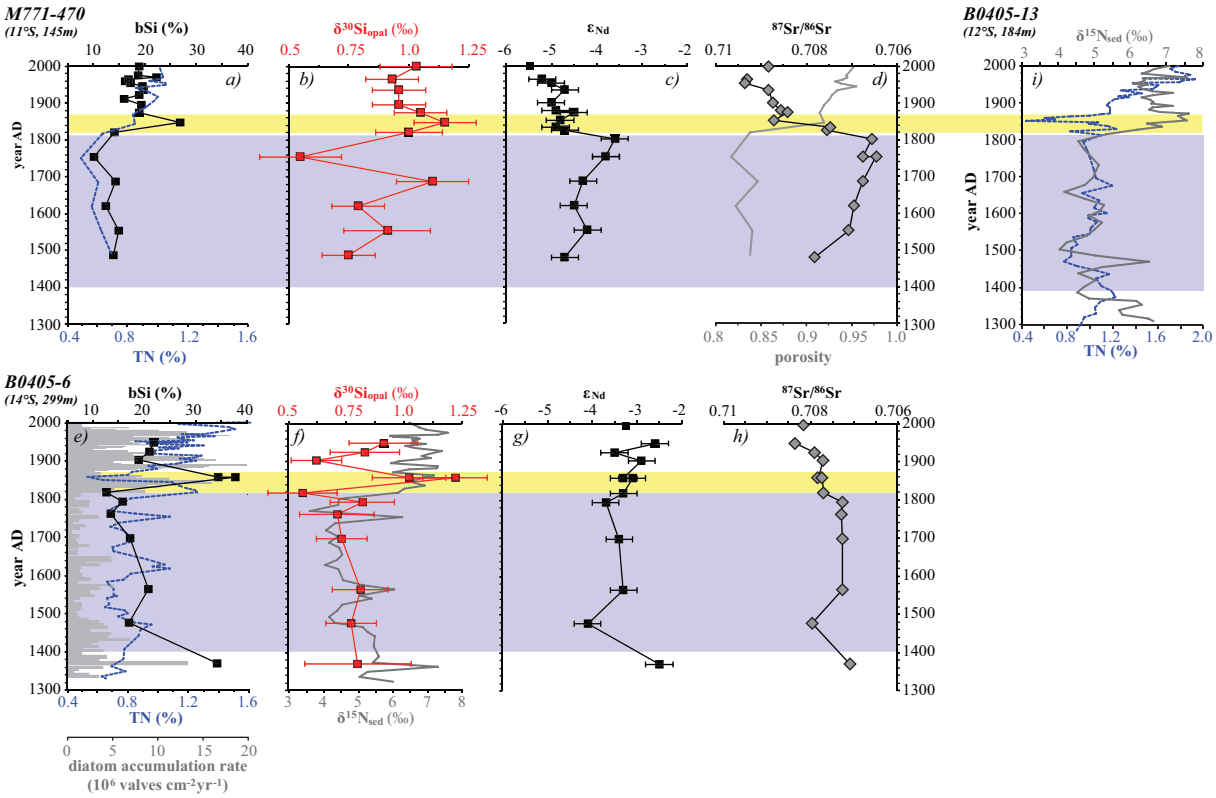

Figure 2. Downcore records for core M771-470 (upper panel) and core B0405-6 (lower panel). The blue and yellow shadings indicate the age range of the LIA and the transitional period, respectively. a/e) bSi concentration (black squares), total N concentration (dashed blue curve), e) diatom accumulation rate (grey bars) (Gutiérrez et al., 2009), b/f) $\delta^{30}Si_{opal}$ (red squares), f) bulk $\delta^{15}N_{sed}$ (grey curve) (Gutiérrez et al., 2009), c/g) $\varepsilon_{Nd\ detritus}$ (black squares), d/h) $^{87}Sr/^{86}Sr_{detritus}$ (grey diamonds, x-axis is inverted), d) sediment porosity (grey curve). Error bars represent $2\sigma_{(sd)}$ external reproducibilities of repeated standard or sample measurements. Panel i) for comparison shows the total N content and $\delta^{15}N_{sed}$ of core B0405-13 (Gutiérrez et al., 2009).

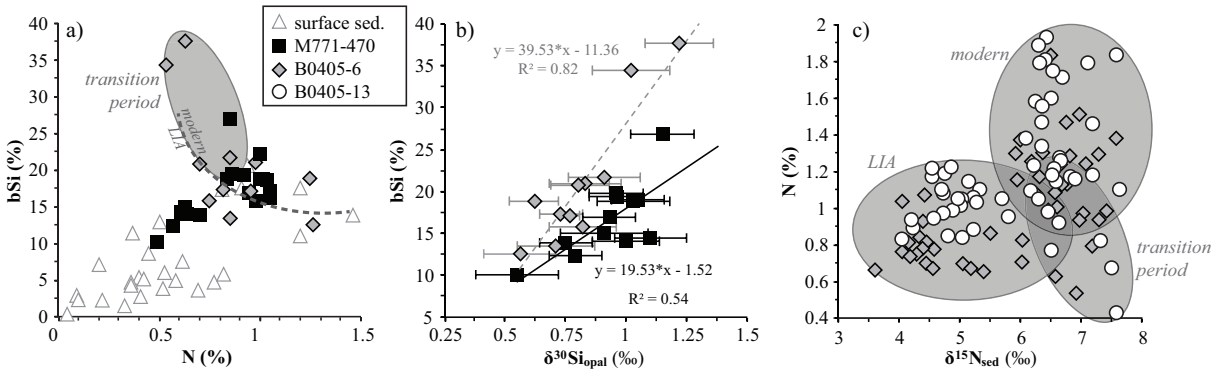

916

917 Figure 3. Surface sediment (white triangles) and downcore data (core M771-470: black
918 squares, B0405-6: grey diamonds, B0405-13: white circles) for a) total N versus bSi
919 concentrations (the dashed line marke the end of the LIA), b) $\delta^{30}Si_{opal}$ versus bSi
920 concentration and c) $\delta^{15}N_{sed}$ versus total N concentrations. Error bars represent $2\sigma_{(sd)}$ external
921 reproducibilities.

922

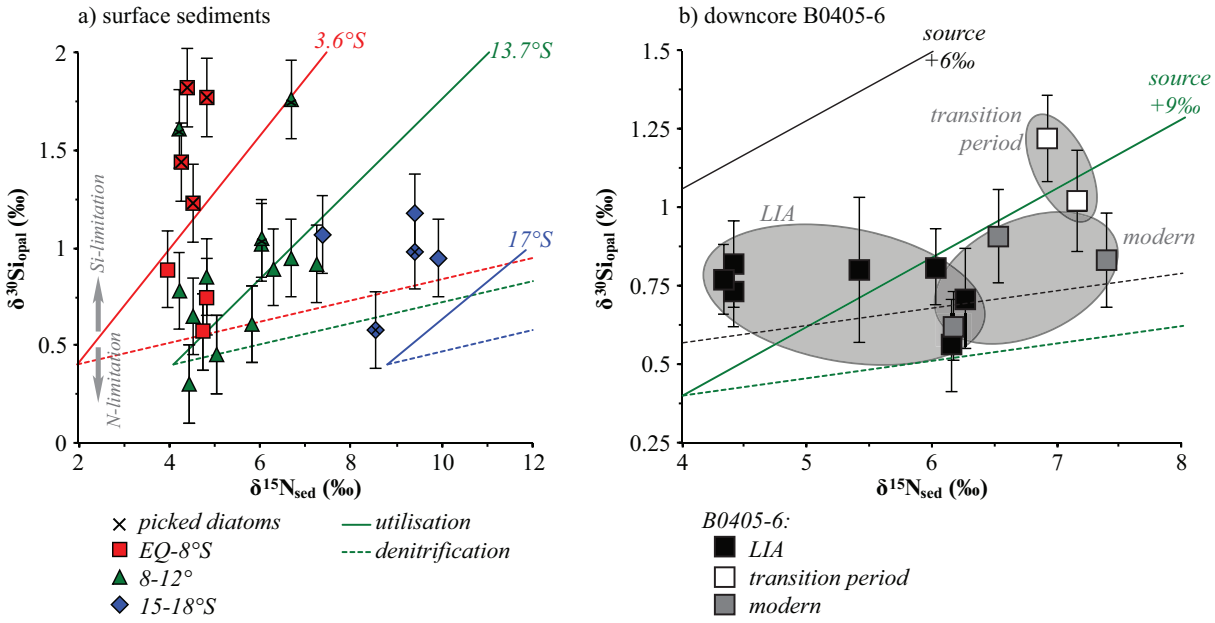

Figure 4. Relationship between $\delta^{15}N_{sed}$ versus $\delta^{30}Si_{opal}$ for a) surface sediments and b) downcore data from core B0405-6. The crosses in a) indicate $\delta^{30}Si$ data obtained from hand-picked diatoms, which reflect a different growth season than bulk $\delta^{30}Si_{opal}$ and which are influenced by stronger $Si(OH)_4$ limitation (higher $\delta^{30}Si$) (Ehlert et al., 2012). The solid lines reflect theoretical utilisation (assuming 1:1 utilisation of $Si(OH)_4$ and NO_3^- by the diatoms) and the dashed lines mark the theoretically expected line for denitrification, which represent the expected signal preserved in the sediments, based on present-day measurements: $\delta^{30}Si$ source signature and enrichment factor $\varepsilon_{diatom\text{-}Si(OH)4}$ are always +1.5‰ (Ehlert et al., 2012) and -1.1‰ (De La Rocha et al., 1997), respectively. $\delta^{15}N_{sed}$ source signature and $\varepsilon_{organic\text{-}NO3\text{-}}$ vary with latitude (Mollier-Vogel et al., 2012), in the north at 3.6°S source signature and ε are +5.7‰ and -3.7‰ (red curves), along the central shelf at 13.7°S source signature and ε are +8.9‰ and -4.8‰ (green curves), and in the south at 17°S source signature and ε were measured to be +14.5‰ and -5.7‰ (blue curves), respectively. The samples are colour-coded according to their location on the shelf and relative to the NO_3^- utilisation/NO_3^--loss that they experienced. Data points that plot above the utilisation curves reflect predominant $Si(OH)_4$ limitation whereas data points below record stronger NO_3^- limitation. The isotopic enrichment during denitrification was always set to be +20‰. For the downcore data (b) two different assumed source signatures are displayed: +9‰ (green lines, corresponding to the modern conditions along the central shelf region in a) and +6‰ (grey lines). Data points are colour-

943 coded according to the respective time periods (black: LIA, white: transition period, grey:
944 modern). Error bars represent $2\sigma_{(sd)}$ external reproducibilities.
945

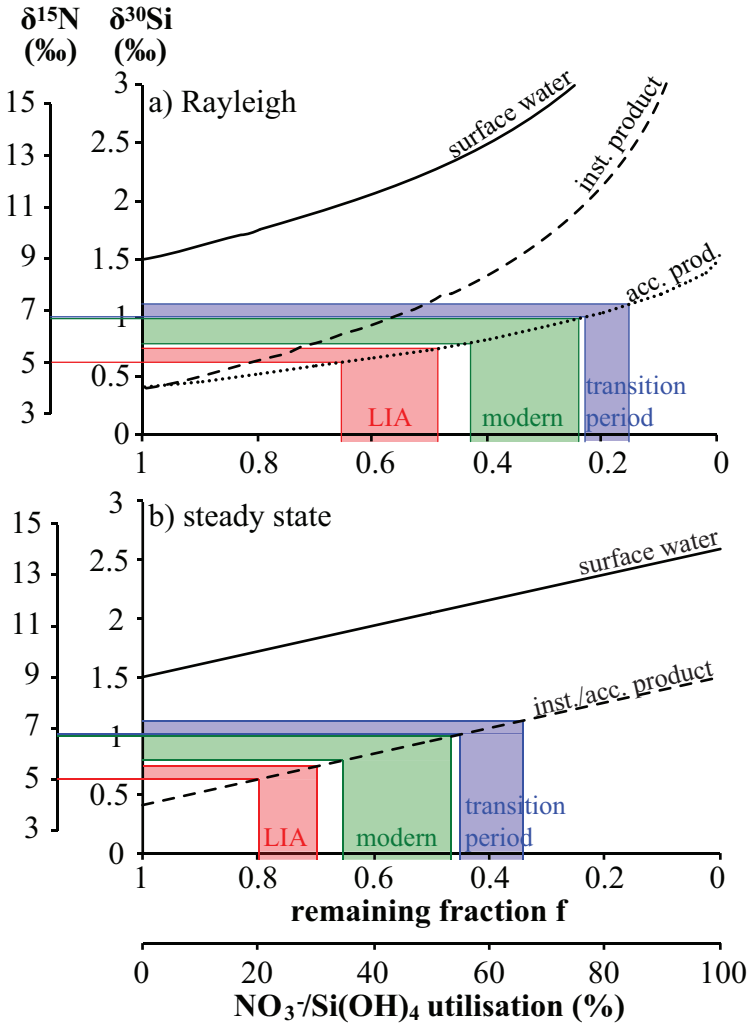

946

947 Figure 5. Theoretical changes in $\delta^{30}Si$ and $\delta^{15}N$ values of seawater and the instantaneous and
948 accumulated product as a function of f (remaining nutrients from the available pool =
949 $[nutrient_{observed}]/[nutrient_{initial}]$) with an initial $\delta^{30}Si_{Si(OH)4}$ value of +1.5‰ and $\delta^{15}N_{NO3-}$ of
950 +9‰. The formation of the product, e.g. diatom opal, follows either a) Rayleigh-type
951 fractionation or b) steady state-type fractionation behaviour, with enrichment factors ε of -
952 1.1‰ ($\delta^{30}Si$) and -5‰ ($\delta^{15}N$) (corresponding to conditions along the modern central Peruvian
953 shelf, see Fig. 4). The colour shadings mark the range of measured mean $\delta^{30}Si_{opal}$ (both cores)
954 and $\delta^{15}N_{sed}$ (B0405-6 only) in the cores for the LIA (red), the transition period (blue) and
955 modern sediments (green), from which the respective nutrient utilisation (%) can be deduced.
956

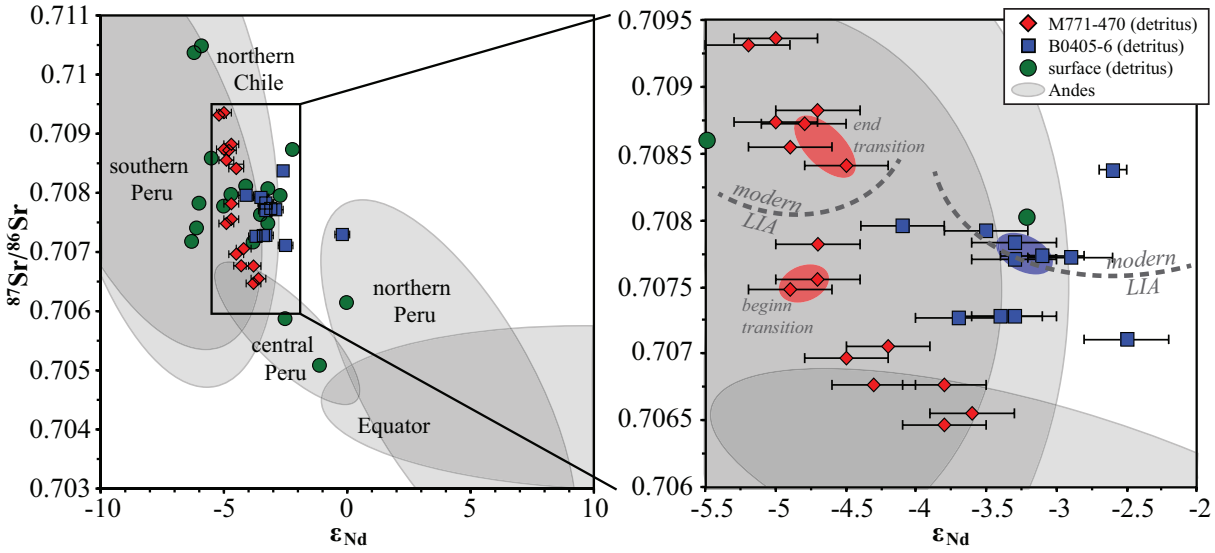

957

958 Figure 6. $\varepsilon_{Nd\ detritus}$ versus $^{87}Sr/^{86}Sr_{detritus}$ for core M771-470 (red diamonds) and B0405-6 (blue
959 squares). Error bars represent $2\sigma_{(sd)}$ external reproducibilities. The green dots are data
960 obtained from surface sediment samples at different sites on the Peruivian shelf. The grey
961 shadings indicate potential sources and provenance endmembers of the detrital material.